Research
A SCIENCE PARTNER JOURNAL

RESEARCH ARTICLE

Significant but Overlooked: Atmospheric HONO Formation from Surface Ammonium Oxidation with Superoxide Radicals

Hong Wang[1,2,3], Zehui Hu[1], Shujun Liu[1], Xin Zhang[1], Meijia Jiang[2], Yanjuan Sun[2,3], and Fan Dong[1,3*]

[1]Research Center for Carbon-Neutral Environmental & Energy Technology, Institute of Fundamental and Frontier Sciences, University of Electronic Science and Technology of China, Chengdu 611731, China. [2]School of Resources and Environmental, University of Electronic Science and Technology of China, Chengdu 611731, China. [3]Key Laboratory of Atmospheric Pollution Causes, Prevention and Control in Complex Terrain of Chengdu-Chongqing Region, Ministry of Ecology and Environment, PRC, Chongqing 401147, China.

*Address correspondence to: dongfan@uestc.edu.cn, dfctbu@126.com

Citation: Wang H, Hu Z, Liu S, Zhang X, Jiang M, Sun Y, Dong F. Significant but Overlooked: Atmospheric HONO Formation from Surface Ammonium Oxidation with Superoxide Radicals. *Research* 2025;8:Article 0819. https://doi.org/10.34133/research.0819

Submitted 4 June 2025
Revised 27 June 2025
Accepted 12 July 2025
Published 12 August 2025

Copyright © 2025 Hong Wang et al. Exclusive licensee Science and Technology Review Publishing House. No claim to original U.S. Government Works. Distributed under a Creative Commons Attribution License (CC BY 4.0).

Resolving the sources of HONO formation is an indispensable aspect in understanding the enhancement of atmospheric oxidation. However, the contributing sources of high HONO formation rate remain unclear during humid haze episodes. The photochemical conversion of surface nitrate (NO_3^-), considered as the dominant contributor to the daytime HONO generation, exhibits severe constraint under high relative humidity (RH) conditions. Unexpectedly, ammonium (NH_4^+) on the surface of photoactive mineral dust shows a gradual acceleration of HONO generation with increasing RH under simulated solar irradiation, especially at high RH. This reversed observation stems from a change in the photochemical pathway for the HONO formation from NO_3^- and NH_4^+. The photochemical conversion of surface NO_3^- is determined by photogenerated electrons ($NO_3^- \rightarrow NO_2 \rightarrow NO_2^- \rightarrow HONO$), while the superoxide radical ($\bullet O_2^-$) generated during photochemical reaction drives the surface NH_4^+ to directly form HONO with the pathway ($NH_4^+ \bullet + \bullet O_2^- \rightarrow NO_2^- + H_2O \rightarrow HONO$). Under high RH conditions, oxygen molecules (O_2) have greatly better access to photogenerated electrons than NO_2, resulting in an interruption of the procedure from NO_2 to NO_2^- during NO_3^- conversion. Therefore, the favorably generated $\bullet O_2^-$ fuels the photochemical conversion of surface NH_4^+ while inhibiting the conversion of NO_3^- to diurnal HONO formation. This work highlights the overlooked contribution of HONO formation from NH_4^+, especially under high RH conditions, and advances the understanding of a renewed role for O_2 in atmospheric chemical processes.

Introduction

In the tropospheric atmosphere, nitrous acid (HONO) roughly contributes to 30% to 50% of the hydroxyl radical (·OH) production, directly leading to increased atmospheric oxidation and secondary aerosol formation [1–3]. Parsing the sources of HONO becomes a priority in evaluating atmospheric ·OH budgets [4,5]. For daytime HONO levels, the heterogeneous conversion of nitrogen dioxide (NO_2) and photolysis of nitrate (NO_3^-) are considered significant contributing pathways, which may also be enhanced on diverse surfaces in the atmosphere, such as sea salt aerosol, soot, mineral dust, and architectural surfaces [6–10]. Notably, it is found that the low reaction rates of HONO formation by dimerization of NO_2 on many environmental surfaces result in a poor explanation for observations [11–13]. Ma et al. [14] reported that the photolysis of NO_3^- on the surface of typical photoactive mineral dust, TiO_2, has a prominent contribution to HONO generation. However, water displays an inhibitory effect on HONO formation from the surface NO_3^- photolysis under high relative humidity (RH) conditions [14]. This is a paradox that high HONO formation rates are determined during humid haze episodes [12,15]. Hence, there should be unknown sources for the daytime HONO budget, particularly in high RH conditions.

Ammonia (NH_3) is an abundant reduced nitrogen species in the atmosphere [16–20]. NH_3 exhibits increasing emissions over the past decades, even up to parts per million (ppmv) levels in highly polluted regions, and has an important effect on the atmospheric reaction [13,21–23]. NH_3 is effective in promoting the hydrolysis reaction of NO_2 to form HONO by theoretical calculation because the energy barrier of NO_2 conversion is lowered dramatically [24,25]. A new pathway has been discovered, where NH_3 assists in the conversion of NO_2 into HONO under ultraviolet light irradiation on urban surfaces, in which NH_3 acts as a hydrogen carrier to facilitate the transfer of hydrogen from H_2O to monomeric NO_2 [12]. In addition, Kebede et al. [26] reported that HONO can be formed directly by NH_3 photooxidation on the TiO_2 surface. This suggests a potential contributing

role of NH_3 to diurnal HONO formation. Regrettably, the conversion of NH_3 to HONO remained unsatisfactory under high RH conditions. When the RH was increased from 40% to 95%, HONO formation was greatly inhibited, with a decrease in the generation amount of about 86% [26]. This likely stems from the NH_3 conversion process being governed by its collision efficiency with the surface, while the competitive occupation of reactive sites by water molecules may significantly hinder the reaction under high RH conditions [27]. Notably, in the atmosphere, NH_3 prefers to form particulate ammonium (NH_4^+) through gas-to-particle conversion, which is further augmented in pollution episodes [28]. As the NH_3 emissions increase, so does the share of NH_4^+ in the atmospheric environment. Moreover, NH_4^+ often combines with NO_3^- in the form of NH_4NO_3 on the particulate surface, particularly in ammonia-rich areas [29,30]. Accordingly, there is a high incidence of NH_4^+ being triggered by photoactive particulates to undergo photochemical conversion. More importantly, in contrast to NH_3, NH_4^+ adsorbed directly on the surface of particulate matter has the potential to diminish the occupation of reaction sites by water molecules. Hence, it is worth exploring whether the NH_4^+ on mineral dust can contribute to HONO formation under high RH conditions.

Herein, the photochemical conversion from NH_4^+ to HONO on the surface of the typical photoactive mineral dust under a variety of RH conditions was discovered and validated as a new pathway. NH_4NO_3, which is the most common ammonium salt in the atmosphere, was chosen as a proxy. Meanwhile, $NaNO_3$, as a representative of atmospheric nitrate salts, was used as a comparison to elucidate the discrepancy between NH_4^+ and NO_3^- contributing to HONO formation. The dynamic evolution of surface NH_4^+ and NO_3^- was scrutinized by in situ diffuse reflectance Fourier transform infrared spectroscopy (DRIFTS). The trapping experiments of active species were combined to resolve the pathways of HONO formation. Under high RH conditions, the role played by oxygen molecules (O_2) was recognized during the photochemical conversion of NH_4^+ and NO_3^- through conditioned experiments, ^{15}N-isotope labeling, and in situ electron paramagnetic resonance (EPR) spectroscopy. This study reveals an overlooked but significant pathway by which NH_4^+ can contribute to atmospheric HONO formation, especially under high RH conditions.

Results and Discussion

HONO production from the photochemical conversion of ammonium

Figure 1A and B displays the time-dependent production of HONO when $NaNO_3$ and NH_4NO_3 are presented on the surface of typical photoactive mineral dust, TiO_2, at 10%, 25%, 45%, and 75% RH. To clearly distinguish the variation trend of HONO production with the increased RH, histograms of product concentrations are also shown in Fig. 1A (right) and B (right). All samples released HONO upon simulated solar light irradiation, and the generated concentration gradually increased when the RH was adjusted from 10% to 45%. This fact owes to the important roles of water molecules in providing hydrogen protons and promoting decomposition [31,32]. However, at a high RH level of 75%, the HONO production from the photochemical conversion of surface $NaNO_3$ sharply declined. This decrease phenomenon was previously attributed to the deliquescence of $NaNO_3$ at 75% RH [14,33]. However, as for NH_4NO_3, its deliquescence point is 62% RH [34,35]. The trend of gradual increase in HONO generation was still maintained for surface NH_4NO_3 when the RH reached 75% (Fig. 1B). These results suggest that there should be an unidentified mechanism dominating the HONO production during the photochemical conversion of surface NH_4NO_3.

Compared with $NaNO_3$, which contains NO_3^- that results in the production of HONO, NH_4NO_3 possesses other sources of nitrogen, i.e., NH_4^+, which may contribute to the release of HONO. The experiment using isotope-labeled NH_4NO_3-$^{15}NH_4^+$ was conducted under high RH conditions (Fig. 1C). The mass spectra of the HONO decomposition product (NO) are similar to that of the standard ^{15}NO, indicating that the nitrogen element in the HONO product can derive from NH_4^+. Subsequently, NH_4OH was used as a single representative of NH_4^+ to load on the TiO_2 surface for photochemical reaction testing. As shown in Fig. 1D, appreciable HONO concentrations were observed during the irradiation at 25%, 45%, and 75% RH. This indicates that the single NH_4^+ itself is available as a new source of daytime HONO.

Furthermore, samples loading both NH_4OH and $NaNO_3$ were investigated to understand the contribution of NH_4^+ and NO_3^- to HONO formation at different RH. As shown in the green shaded area of Fig. 1D, there is an additional HONO concentration in comparison to the pure NH_4OH sample. Moreover, the green shaded area was enlarged as the RH increased from 25% to 45% (Fig. 1D), which is consistent with the phenomenon in Fig. 1A that the photochemical conversion of surface NO_3^- to HONO can be facilitated by water molecules in the moderate RH range. Notably, at a high RH level of 75%, there was hardly a green shaded area. Pure NH_4OH and NH_4OH/$NaNO_3$ mixture samples generated nearly identical HONO concentrations under irradiation. These results consolidate that, under high RH conditions, the photochemical conversion of surface NO_3^- may be a relatively weak contribution to HONO production in the atmosphere. Conversely, NH_4^+ is probably the vital benefactor to the enhanced atmospheric oxidation capacity during haze pollution, especially under high RH conditions.

To verify the generalization of the above results to the atmospheric environment, the photochemical conversion of $NaNO_3$ and NH_4NO_3 was further carried out on the surface of authentic mineral dust (A1 dust) under simulated solar light. As shown in Fig. 1E and F, as the RH changes from 45% to 75%, the HONO formation presented a declining tendency for the photochemical conversion of $NaNO_3$, while an increasing trend was still maintained for that of NH_4NO_3. Therefore, abundant NH_4^+, which is commonly coexisting with NO_3^- on the surface of photoactive mineral dust, may be a seriously overlooked source of daytime HONO in the atmospheric environment, especially under high RH conditions. As shown in Fig. 1G, in addition to the photochemical conversion of surface NO_3^- (pathway I), there should be a new pathway of surface NH_4^+ contributing to daytime HONO formation in the atmosphere (pathway II).

HONO formation mechanisms for photochemical conversion of ammonium

To understand the HONO generation pathways, in situ DRIFTS was employed to investigate the dynamic evolution of surface NO_3^- and NH_4^+ under light irradiation at low (10%) and high (75%) RH. For the surface $NaNO_3$ sample under low RH conditions (Fig. S1), once the light was started, the observed variation in infrared spectra was the NO_2 (1,626 cm^{-1}), NO_2^- (1,426 cm^{-1}), and NO_3^- (1,578, 1,570, 1,296, and 1,259 cm^{-1}) bands [32,36–38].

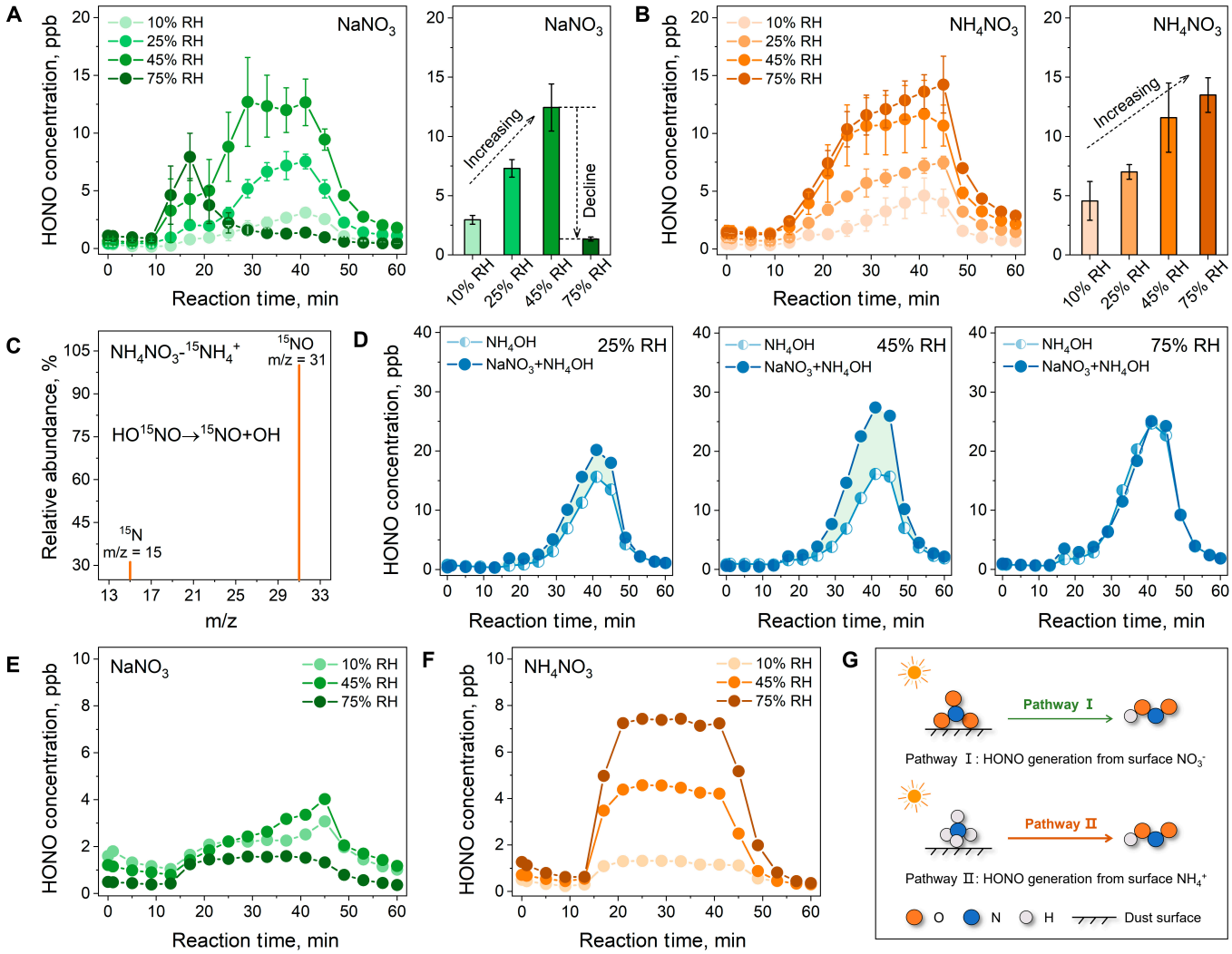


Fig. 1. HONO generation evaluation for photochemical conversion of surface NO_3^- and NH_4^+ at different RH conditions: HONO formation from $NaNO_3$ (A, left) and NH_4NO_3 (B, left) adsorbed on TiO_2 surface with time of illumination at different RH conditions. The histograms represent the concentrations of HONO formation from $NaNO_3$ (A, right) and NH_4NO_3 (B, right) at 30 min of illumination. Gas chromatography–mass spectrometry spectra of the HONO decomposition product (NO) from the photochemical conversion of NH_4NO_3-$^{15}NH_4^+$ at high RH conditions (C). HONO formation from NH_4OH and $NaNO_3$ + NH_4OH mixture adsorbed on TiO_2 surface under simulated solar irradiation at 25% RH, 45% RH, and 75% RH conditions (D). HONO formation from $NaNO_3$ (E) and NH_4NO_3 (F) adsorbed on the A1 dust surface under simulated solar irradiation at different RH conditions. (G) Diagram of the HONO formation pathway from surface NO_3^- and NH_4^+.

Among them, NO_2 and NO_2^- belong to the products of photochemical NO_3^- conversion, while the generated NO_3^- is due to the re-oxidation of photochemical products by active species, such as h^+, $\cdot O_2^-$, and ·OH [39,40]. The peak intensity is enhanced progressively with increasing light duration. The accumulation of NO_3^- is particularly prominent. This suggests that most of the photochemical products are forced to be re-oxidized to NO_3^- at low RH, due to the shortage of water molecules on the surface. Similar products and evolution were found during the photochemical conversion of NH_4OH (Fig. S2) and NH_4NO_3 (Fig. S3) under low RH conditions. Therefore, it is inferred that the photochemical conversion of both NO_3^- and NH_4^+ requires water molecules to provide adequate hydrogen protons for the hydrogenation reactions to achieve HONO formation.

At high RH conditions, the photochemical products of the samples are consistent with those under low RH (Fig. 2A to C). Differently, as shown in Fig. 2A, the depletion of the surface NO_3^- band at 1,357 cm^{-1} and the generation of NO_2^- band at 1,430 cm^{-1} became evident during the photochemical NO_3^- conversion. The peak intensity of generated NO_3^- (1,568, 1,298, and 1,261 cm^{-1}) also moderated. These facts suggest that adequate water molecules advance the surface NO_3^- conversion and slow down the re-oxidation of photochemical products. Generally, the photochemical conversion occurring on the surface of photoactive particulate matter is primarily driven by the generated active species [39,41]. Under light irradiation, photogenerated electrons and holes are derived from photoexcitation of photoactive particulate matter. Then, the generated electrons reduce O_2 to $\cdot O_2^-$ and holes oxidize H_2O to ·OH. As shown in Figs. S4 to S6, the photogenerated carriers, $\cdot O_2^-$, and ·OH were detected in the TiO_2 sample under light conditions. To further confirm the key active species that drive the photochemical conversion of surface NO_3^-, we performed corresponding capture experiments. As shown in Fig. 2D, under both humidity conditions, there was a significant inhibition of HONO production only after the photogenerated electrons were captured, demonstrating that photogenerated

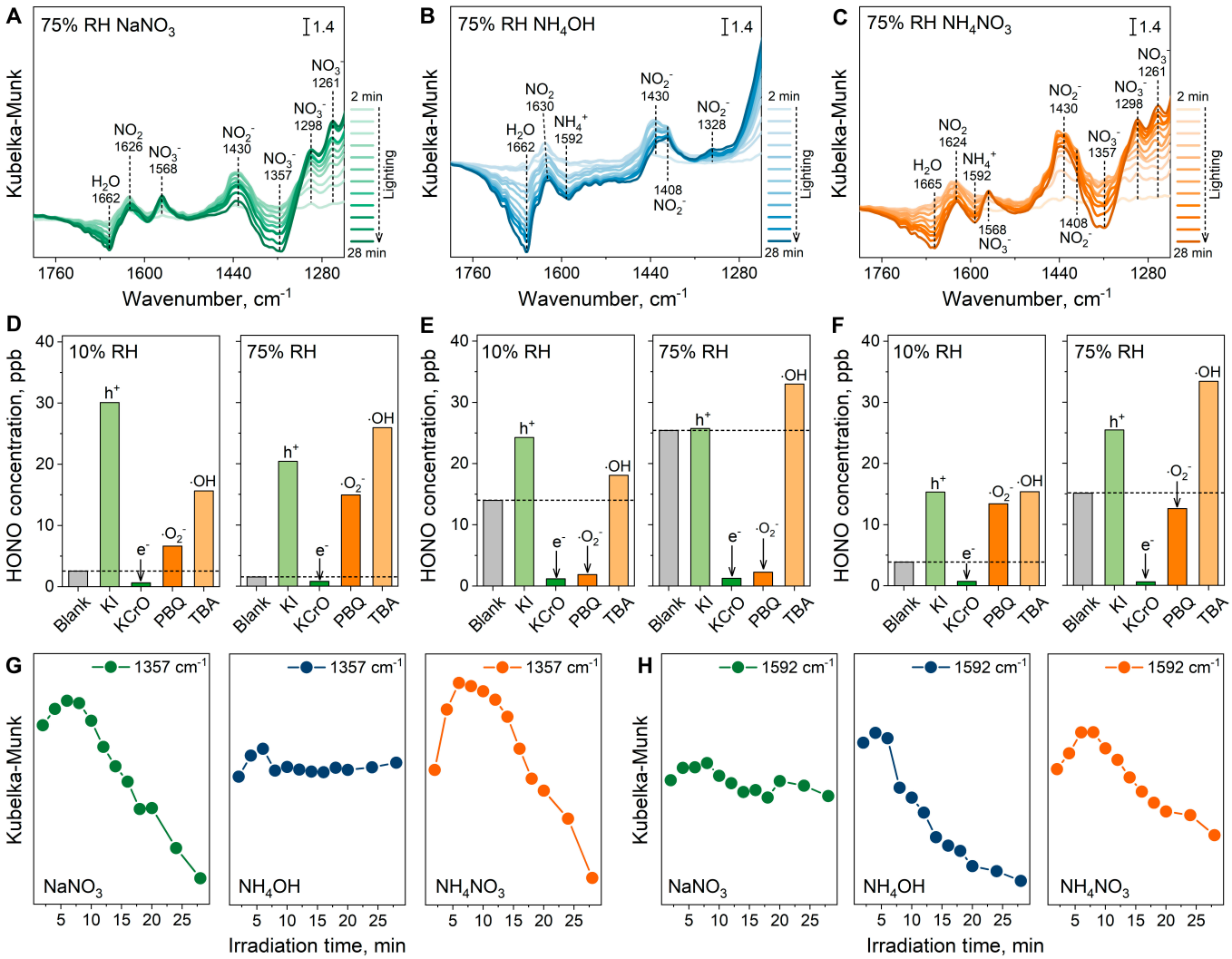


Fig. 2. Dynamic evolution and radical trapping for surface NO_3^- and NH_4^+: In situ DRIFTS of $NaNO_3$ (A), NH_4OH (B), and NH_4NO_3 (C) adsorbed on the TiO_2 surface under simulated solar irradiation at 75% RH. The variation of HONO-generating concentrations of $NaNO_3$ at 10% (D, left) RH and 75% RH (D, right), NH_4OH at 10% (E, left) RH and 75% RH (E, right), and NH_4NO_3 at 10% (F, left) RH and 75% RH (F, right) with trapping experiments of active species. The detailed evolution of the NO_3^- peak with time at 1,357 cm^{-1} (G) and NH_4^+ peak with time at 1,592 cm^{-1} (H) in infrared spectra of $NaNO_3$, NH_4OH, and NH_4NO_3.

electrons are the crucial driver of the photochemical NO_3^- conversion. Coupled with the detected intermediates in Fig. 2A and their valence state of nitrogen element, the photochemical conversion pathway from NO_3^- to HONO is reasoned to be $NO_3^- \rightarrow NO_2 \rightarrow NO_2^- \rightarrow$HONO, as shown in Eqs. 1 to 3. The other active species serve primarily to re-oxidize the photochemical products to NO_3^- (Eq. 4) so that, after trapping them, more HONO can be monitored. Besides, the accumulation of NO_3^- can be observed in the infrared spectrum (Fig. 2A).

$$NO_3^- + e^- \rightarrow NO_2 + O^- \quad (1)$$

$$NO_2 + e^- \rightarrow NO_2^- \quad (2)$$

$$NO_2^- + H_2O \rightarrow HONO + OH^- \quad (3)$$

$$NO_2/NO_2^- + h^+/\cdot O_2^-/OH \rightarrow NO_3^- \quad (4)$$

As for the surface NH_4OH sample under high RH conditions (Fig. 2B), with increasing light time, the characteristic peak belonging to NH_4^+ at 1,592 cm^{-1} was consumed significantly [42]. Meanwhile, the peaks of NO_2 at 1,630 cm^{-1} and NO_2^- at 1,430, 1,408, and 1,328 cm^{-1} emerged, suggesting that NH_4^+ mainly undergoes a photooxidation process. Notably, the conversion of NH_4^+ to HONO was greatly hindered when either photogenerated electrons or $\cdot O_2^-$ was captured (Fig. 2E). Given that the generation of $\cdot O_2^-$ also requires the presence of photogenerated electrons (Eq. 5), the role of photogenerated electrons and $\cdot O_2^-$ for the photochemical conversion of NH_4^+ was further identified. The NH_4OH sample was subjected to continuous-flow daylight tests in an argon (oxygen-free) atmosphere at 75% RH. As shown in Fig. S7, the HONO formation became almost negligible. This result demonstrated that, for the photochemical conversion of NH_4^+ to HONO, the oxygen (O_2) is the essential driver, which acquires photogenerated electrons to form $\cdot O_2^-$ and then gradually oxidizes NH_4^+ to NO_2^-. It is unfortunate that more transient intermediates were not monitored, possibly due to the rapidity of the reaction or the

overlap of the spectral region [26,43]. According to the generation of NO_2^- in Fig. 2B, the total reaction for the conversion of NH_4^+ to NO_2^- driven by $\cdot O_2^-$ is shown in Eq. 6. Significantly, there is a great difference in the photochemical conversion pathways of NH_4^+ and NO_3^-. The photochemical pathway of NH_4^+ is $NH_4^+ \rightarrow NO_2^- \rightarrow$HONO. $\cdot O_2^-$ is used for the NH_4^+ conversion, and adequate water molecules available for NO_2^- to HONO formation mitigate the re-oxidation of photochemical products, so the accumulated NO_3^- peaks hardly appeared in Fig. 2B. Besides,

$$O_2 + e^- \rightarrow \cdot O_2^- \quad (5)$$

$$NH_4^+ + 2 \cdot O_2^- \rightarrow NO_2^- + 2H_2O \quad (6)$$

For the surface NH_4NO_3 sample, its infrared spectra exhibited photochemical conversion characteristics of both species, NO_3^- and NH_4^+, under high humidity conditions (Fig. 2C). Detailly, as shown in Fig. 2G and H, the depletion that is unique to NO_3^- (1,357 cm^{-1}) in the surface $NaNO_3$ sample and NH_4^+ (1,592 cm^{-1}) in the surface NH_4OH sample was observed in the surface NH_4NO_3 sample. This indicates that the photochemical conversion processes of NO_3^- and NH_4^+ are occurring simultaneously in the surface NH_4NO_3 sample. Correspondingly, when photogenerated electrons were quenched, the HONO formation was significantly suppressed (Fig. 2F). When $\cdot O_2^-$ was quenched, surface NH_4NO_3 allowed decent HONO formation at low RH conditions. This is because, although the photochemical conversion of NH_4^+ struggles, some NO_3^- photochemical products also escape $\cdot O_2^-$ re-oxidization to participate in HONO generation. Notably, under high RH, photochemical conversion from NH_4NO_3 to HONO displayed depression after $\cdot O_2^-$ quenching, reaffirming that the surface NO_3^- conversion is restricted and surface NH_4^+ becomes the main contributing source of daytime HONO level.

Effect of O_2 on the photochemical conversion from ammonium to HONO

To sum up, as shown in Fig. 3A, the photochemical conversion of surface NH_4^+ is mainly driven by $\cdot O_2^-$, whereas that of surface NO_3^- relies on photogenerated electrons. Furthermore, the dynamic evolution of the critical species (NO_2^-) during the NH_4^+ and NO_3^- conversion was dissected to elucidate the cause of their difference in HONO production under high RH conditions. As shown in Fig. 3B (left), although NO_3^- was able to generate a certain amount of NO_2^- in the early stage, the surface NO_2^- was rapidly reduced by 85.3% to near depletion as the light reaction proceeded. Differently, the accumulation of NO_2^- during the conversion of surface NH_4NO_3 nearly doubled, and a favorable production–consumption equilibrium was maintained, with a declining amount of only 21.9% as the reaction progressed (Fig. 3B, right). Accordingly, when adequate water molecules are present, NH_4NO_3 can induce the formation of enough NO_2^- for HONO production, whereas $NaNO_3$ cannot. Curiously, the depletion of surface NO_3^- was occurring as usual during photochemical conversion (Fig. 2G). The other reactive nitrogen species were monitored when surface $NaNO_3$ was irradiated at 75% RH. As shown in Fig. S8, unlike the case of HONO production, surface $NaNO_3$ generated appreciable amounts of NO_2 under high RH, suggesting that the conversion from NO_3^- to NO_2 is smooth. Hence, it can be inferred that the inability of NO_3^- to HONO is mainly derived from the hindered NO_2^- generation at the step of NO_2 gaining electrons ($NO_2 + e^- \rightarrow NO_2^-$).

During photochemical reactions, for NO_2, O_2 may be a formidable competitor for expending photogenerated electrons, as it tends to be activated to form $\cdot O_2^-$. In situ EPR was applied to investigate whether O_2 has a superior ability to acquire photogenerated electrons than NO_2 on the surface [44]. Under exposure to light, the TiO_2 sample produces abundant photogenerated electrons, so a greatly enhanced EPR signal intensity emerged (Fig. S9). Subsequently, the NO_2 atmosphere was introduced into the in situ reaction chamber. A slight decrease in EPR signal intensity ($\Delta = 0.15$) can be seen in Fig. 3C, indicating that a part of the photogenerated electrons has been consumed by NO_2. When water molecules were present in the introduced NO_2 atmosphere, the consumption of photogeneration electrons by NO_2 was not promoted, and the decrease in the EPR signal intensity remained at 0.15 (Fig. 3D). Prominently, when the O_2 atmosphere was introduced, the intensity of the EPR signal drop reached 0.27 (Fig. 3F). This result proves that O_2 indeed has a greater ability to acquire photogenerated electrons than NO_2. Meanwhile, the EPR signal belonging to $\cdot O_2^-$ appeared, indicating that O_2 is activated to form $\cdot O_2^-$ after capturing the photogenerated electron [45]. The O_2 atmosphere accompanying the water molecules was also investigated. Surprisingly, as shown in Fig. 3J, the more significant photogenerated electron consumption appeared ($\Delta = 0.38$), along with a stronger EPR signal belonging to $\cdot O_2^-$. This result manifests that water molecules can greatly enhance the acquisition of photogenerated electrons by O_2. Accordingly, during photochemical reactions, O_2 enables the consumption of photogenerated electrons in preference to NO_2, which is further exacerbated under high RH conditions. This variation may result in the inability of NO_2 to efficiently obtain photogenerated electrons for the conversion to NO_2^- under high RH conditions, thereby interrupting the HONO formation from surface NO_3^-.

To identify the inhibitory effect of O_2 on the photochemical conversion of NO_3^-, the daylight tests of samples were placed in an argon atmosphere at 75% RH. As shown in Fig. 3E, decent HONO production appeared. These results confirmed that, under high RH, O_2 significantly inhibits the acquisition of photogenerated electrons by NO_2, resulting in the inability of NO_2^- production, and then restricts photochemical conversion from NO_3^- to HONO. Besides, the generated $\cdot O_2^-$ will re-oxidize the photochemical products to NO_3^-, which also retards the production of HONO. However, the NH_4^+ pathway requires O_2 to acquire photogenerated electrons. The generated $\cdot O_2^-$ is the indispensable driver for HONO formation during the photochemical conversion of NH_4^+. Therefore, as shown in Fig. 3H, O_2 inhibits the conversion of NO_3^- and drives the contribution of NH_4^+ to HONO formation under high humidity conditions. The great contribution of NH_4NO_3 to HONO formation under air atmosphere mainly derives from the photochemical conversion of surface NH_4^+, whereas that under argon atmosphere stems from surface NO_3^-.

Universality of the photochemical conversion from ammonium to HONO driven by $\cdot O_2^-$

As a result, daytime HONO formation pathways from surface NO_3^- and NH_4^+ are shown in Fig. 4. In pathway I, photogenerated electrons are generated on the surface of photoactive mineral dust under solar irradiation, which can trigger the

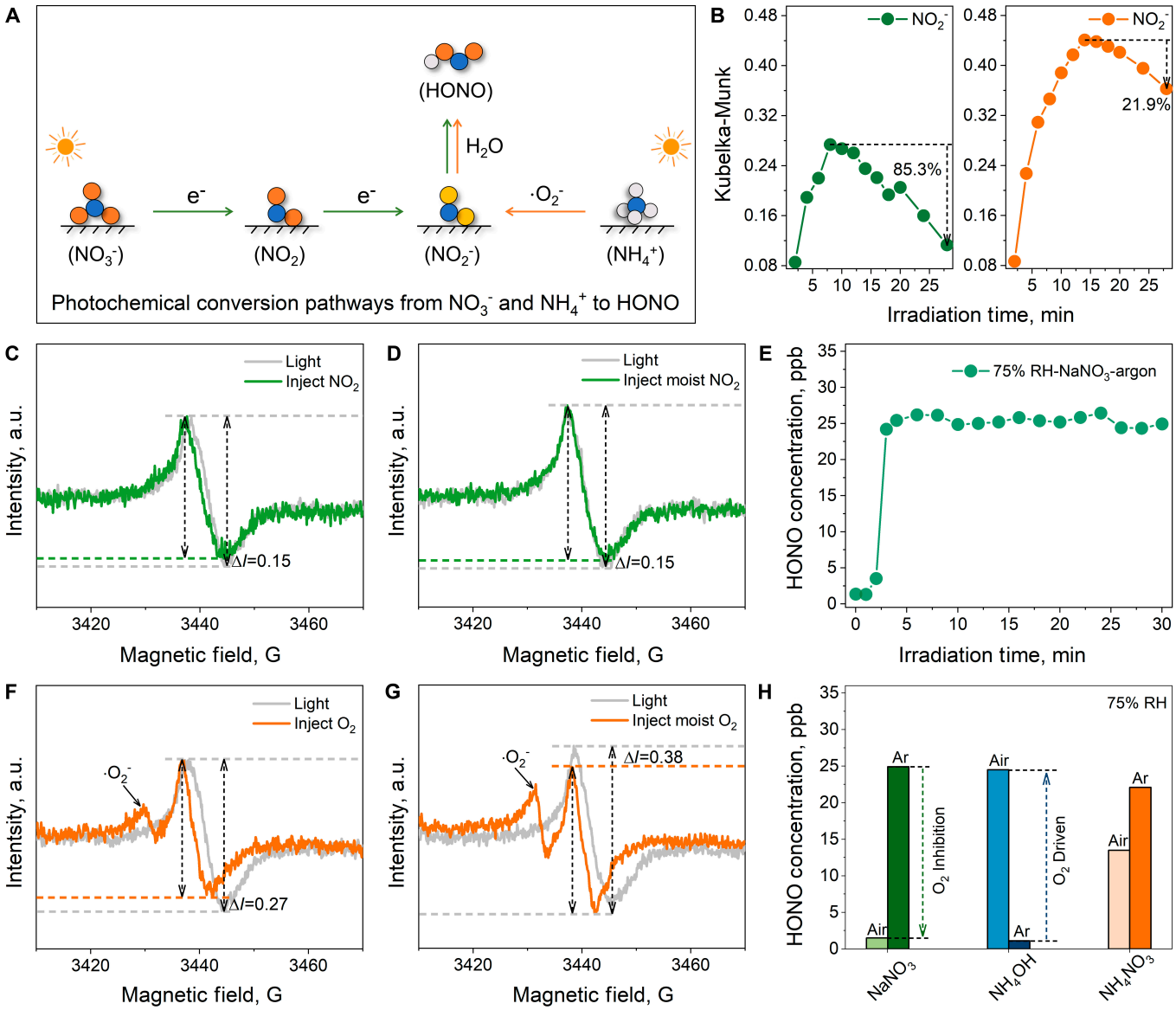


Fig. 3. Reaction mechanism for photochemical conversion of surface NH_4^+ driven by $\cdot O_2^-$. (A) Diagram of photochemical conversion pathways from surface NO_3^- and NH_4^+ to HONO. (B) Detailed evolution of the NO_2^- peak in infrared spectra of $NaNO_3$ and NH_4NO_3. In situ EPR of NO_2 (C) and moist NO_2 (D). HONO formation from $NaNO_3$ and NH_4NO_3 adsorbed on TiO_2 surface under simulated solar irradiation at 75% RH conditions in argon atmosphere (E). In situ EPR of O_2 (F) and moist O_2 (G). HONO formation from $NaNO_3$, NH_4OH, and NH_4NO_3 adsorbed on TiO_2 surface under simulated solar irradiation at 75% RH conditions in air and argon atmosphere (H).

step-by-step conversion of surface NO_3^- to produce HONO (NO_3^-→NO_2→NO_2^-→HONO). In the air atmosphere, O_2 competitively consumes photogenerated electrons to hinder photochemical conversion from surface NO_3^- to HONO, especially under high RH conditions. Differently, in pathway II, $\cdot O_2^-$ drives the photochemical conversion of NH_4^+ to produce HONO ($NH_4^+ + \cdot O_2^- \rightarrow NO_2^- + H_2O \rightarrow$HONO), where photogenerated electrons are mainly responsible for the reduction of O_2 to form $\cdot O_2^-$. This is distinct from the previously reported pathway for the photo-oxidation of NH_3 to generate HONO, which is derived from the reduction of NO_2, where NO_2 is the product of the water-catalyzed oxidation of NH_3 (NH_3→NO_2→HONO) [26]. Significantly, NH_4^+ has a superior contribution to daytime HONO formation under high RH conditions, because the $\cdot O_2^-$ generation is promoted by water molecules.

To demonstrate that the photochemical conversion from NH_4^+ to HONO was extensive in the atmosphere, the HONO generation from surface $(NH_4)_2SO_4$ and NH_4Cl, the proxy for atmospheric ammonium salts, was investigated. As shown in Fig. S10, under solar light irradiation, $(NH_4)_2SO_4$ and NH_4Cl also undergo photochemical conversion to produce HONO at high RH conditions. Particularly, when $\cdot O_2^-$ was trapped during the photochemical conversion of surface $(NH_4)_2SO_4$ and NH_4Cl, their HONO generation was significantly inhibited, suggesting that the $\cdot O_2^-$-driven photochemical conversion from surface NH_4^+ to HONO was universal at high RH in the atmosphere. This finding aligns with field observations during humid haze episodes in China, where elevated HONO levels often coincide with high RH and substantial particulate ammonium concentrations [46,47]. Therefore, the proposed mechanism involving photochemical conversion of surface NH_4^+ may provide a

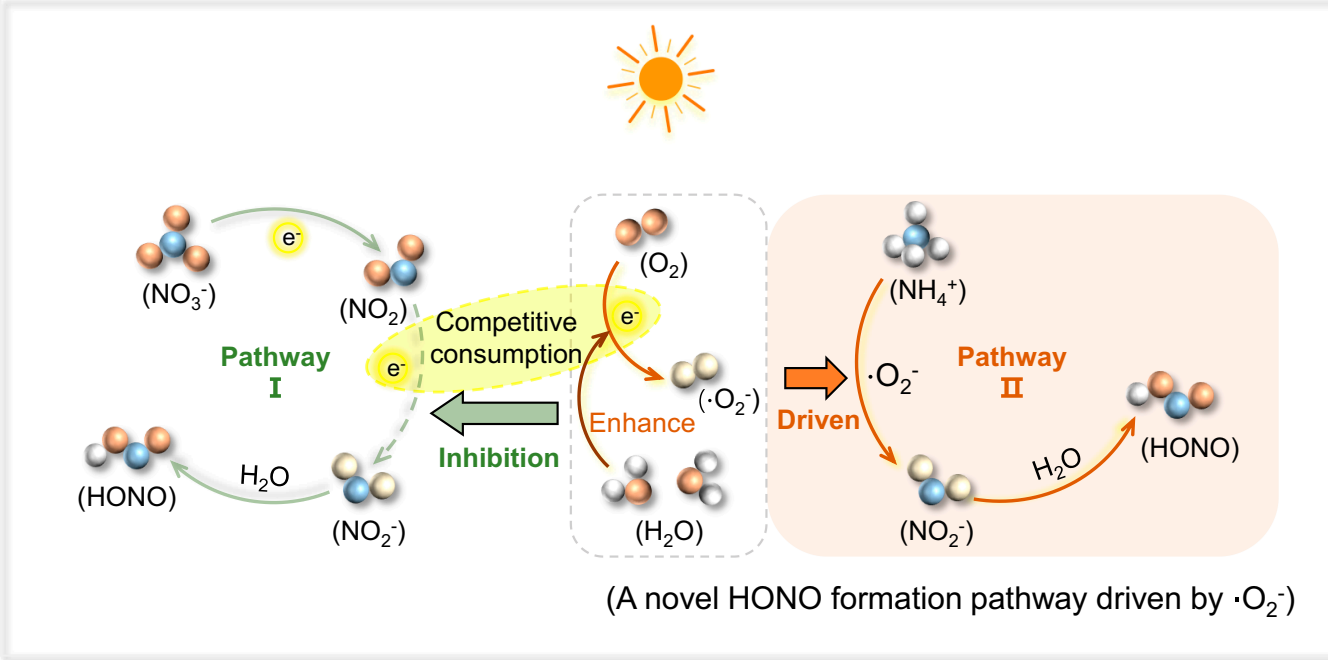


Fig. 4. The schematic illustration for the opposite roles of O_2 during photochemical conversion from NO_3^- and NH_4^+ to HONO.

supplementary explanation for these observations and should be considered in future atmospheric models. Furthermore, for strategies to control NH_4^+ and HONO in regions with high ammonia emissions, in addition to reducing ammonia emissions to minimize NH_4^+ formation, inhibition of aerosol-phase photochemical reactions may be effective in suppressing the generation of interfacial HONO, e.g., by limiting the ambient RH or passivating reactive surfaces to reduce the generation of $\cdot O_2^-$. It is worth noting that the actual atmospheric conditions involve more complexity. Further work is needed to assess the effects of conditions, including aerosol phase and acidity, on HONO formation to develop control strategies.

Conclusion

A significant but overlooked pathway for the daytime HONO formation from the photochemical conversion of NH_4^+ is validated on the surface of atmospheric photoactive mineral dust. Significantly, under high RH conditions, the contribution of surface NH_4^+ to HONO is prominent when that of surface NO_3^- to HONO is substantially suppressed. This discovery could account for the high HONO formation rate during humid haze episodes. The difference in the photochemical HONO formation pathways from surface NH_4^+ and NO_3^- is revealed by in situ DRIFTS and capture experiments. The photochemical conversion of surface NH_4^+ is mainly driven by the generation of $\cdot O_2^-$ after the acquisition of photogenerated electrons by O_2, while NO_3^- directly relies on the gradual reduction of photogenerated electrons. Furthermore, the results of controlled experiments and in situ EPR clarify the opposite roles of O_2 during the HONO formation from NH_4^+ and NO_3^- under high RH conditions. O_2 excels at capturing electrons to generate $\cdot O_2^-$, which can be further enhanced by water molecules, advancing the elevated contribution of NH_4^+ to HONO formation. However, for photochemical conversion of surface NO_3^- under high humidity conditions, the step of NO_2 acquiring photogenerated electrons is highly hindered by the competitive consumption of O_2 to interrupt the path from NO_3^- to HONO. Besides, the $\cdot O_2^-$ generated during the photochemical conversion of NO_3^- will re-oxidize its photochemical products and inhibit the HONO formation. This overlooked and universal pathway from NH_4^+ to HONO would greatly contribute to the enhancement of atmospheric oxidation under high humidity conditions, which sheds light on the significant role of O_2 in atmospheric HONO formation.

Materials and Methods

Materials

All chemical reagents were of analytical grade and were used in this study without further purification. The commercial TiO_2 (typical photoactive components of mineral dust), sodium nitrate ($NaNO_3$), ammonium nitrate (NH_4NO_3), and ammonia (NH_4OH) were obtained from Sigma-Aldrich. Authentic mineral dust (A1 dust) stems from Arizona Test Dust, the detailed components of which are in the Supplementary Materials.

Gas-phase product detection

The gas-phase product concentration during the photochemical conversion was monitored in real time by using a HONO analyzer (HONO-WLPAP) and a NOx analyzer (Thermo, model 42i-TL). The sample with 0.10 g of mineral dust and 0.001 g of nitrate or ammonium was homogeneously dried in Petri dishes. The reaction sample was placed in a rectangular reactor sealed with quartz glass. When clean air or argon gas at a flow rate of 1.5 l/min clears the atmosphere in the reaction chamber, the tungsten halogen lamp was used as simulated solar light to trigger the photochemical reaction. The RH in the photochemical reaction was regulated by a humidity generator (FD-HG). The trapping experiments were performed when the trapping agent of the active species was added to the sample. Photogenerated hole trapping, photogenerated electron trapping, superoxide

radical ($\cdot O_2^-$) trapping, and hydroxyl radical (·OH) trapping were achieved by adding potassium iodide (KI), potassium dichromate ($K_2Cr_2O_7$, short for KCrO), p-benzoquinone (PBQ), and tert-butanol (TBA), respectively.

Photochemical process characterization

The active species, including photogenerated carriers (electrons and holes), $\cdot O_2^-$, and ·OH, were detected by spin-trapped EPR (Bruker EMX nano) spectrometer using 2,2,6,6-tetramethylpiperidine-1-oxyl (TEMPO) and 5,5-dimethyl-1-pyrroline N-oxide (DMPO). The interaction between the photogenerated electron and the reactant molecules was measured by the in situ EPR spectrometer. The photochemical evolution of nitrate (NO_3^-) or ammonium (NH_4^+) on the surface of photoactive mineral dust was monitored using in situ diffuse reflection infrared Fourier transform spectrum (in situ DRIFTS, Bruker INVENIO-R). The detailed description of in situ EPR and in situ DRIFTS was provided in the Supplementary Materials.

Acknowledgments

Funding: This work was supported by the National Natural Science Foundation of China (22225606, 2240060281, and 22261142663), Sichuan Province Science and Technology Plan (2025NSFTD0003), China National Postdoctoral Program for Innovative Talents (BX20230058), and China Postdoctoral Science Foundation (2024M750359).
Author contributions: F.D. and H.W. conceived the idea and designed this study. Z.H. prepared the samples, conducted characterizations, and performed gas-phase product tests. S.L., X.Z., and M.J. helped analyze the experimental data. H.W., Y.S., and F.D. wrote the paper. All authors discussed the results and edited the paper.
Competing interests: The authors declare that they have no competing interests.

Data Availability

All data needed for this study are available in the article and its Supplementary Materials.

Supplementary Materials

Experimental Description
Figs. S1 to S10

References

1. Cheng Z, Shrivastava M, Ijaz A, Veghte D, Vandergrift GW, Tseng K-P, Lata NN, Kew W, Suski K, Weis J, et al. Enhanced light absorption for solid-state brown carbon from wildfires due to organic and water coatings. *Nat Commun*. 2024;15(1):10326.
2. Zhang W, Tong S, Jia C, Wang L, Liu B, Tang G, Ji D, Hu B, Liu Z, Li W, et al. Different HONO sources for three layers at the urban area of Beijing. *Environ Sci Technol*. 2020;54(20):12870–12880.
3. Li X, Gligorovski S, Herrmann H. Underestimated contribution of HONO to indoor OH radicals: An emerging concern. *Sci Bull*. 2018;63(21):1383–1384.
4. Martins-Costa MTC, Anglada JM, Francisco JS, Ruiz-López MF. The aqueous surface as an efficient transient stop for the reactivity of gaseous NO2 in liquid water. *J Am Chem Soc*. 2020;142(50):20937–20941.
5. Liu S, Wang H, Hu Z, Zhang X, Sun Y, Dong F. Resolving the overlooked photochemical nitrophenol transformation mechanism induced by nonradical species under visible light. *Proc Natl Acad Sci USA*. 2024;121(30):Article e2401452121.
6. Ye C, Zhou X, Pu D, Stutz J, Festa J, Spolaor M, Tsai C, Cantrell C, Mauldin RL, Campos T, et al. Rapid cycling of reactive nitrogen in the marine boundary layer. *Nature*. 2016;532(7600):489–491.
7. Baergen AM, Donaldson DJ. Photochemical renoxification of nitric acid on real urban grime. *Environ Sci Technol*. 2013;47(2):815–820.
8. Ye C, Gao H, Zhang N, Zhou X. Photolysis of nitric acid and nitrate on natural and artificial surfaces. *Environ Sci Technol*. 2016;50(7):3530–3536.
9. Ma Q, Chu B, He H. Revealing the contribution of interfacial processes to atmospheric oxidizing capacity in haze chemistry. *Environ Sci Technol*. 2024;58(14):6071–6076.
10. Wang F, Wang W, Wang Z, Zhang Z, Feng Y, Russell AG, Shi G. Drivers of $PM_{2.5}$-O_3 co-pollution: From the perspective of reactive nitrogen conversion pathways in atmospheric nitrogen cycling. *Sci Bull*. 2022;67(18):1833–1836.
11. Xia D, Zhang X, Chen J, Tong S, Xie H-b, Wang Z, Xu T, Ge M, Allen DT. Heterogeneous formation of HONO catalyzed by CO_2. *Environ Sci Technol*. 2021;55(18):12215–12222.
12. Liu J, Li B, Deng H, Yang Y, Song W, Wang X, Luo Y, Francisco JS, Li L, Gligorovski S. Resolving the formation mechanism of HONO via ammonia-promoted photosensitized conversion of monomeric NO_2 on urban glass surfaces. *J Am Chem Soc*. 2023;145(21):11488–11493.
13. Ge S, Wang G, Zhang S, Li D, Xie Y, Wu C, Yuan Q, Chen J, Zhang H. Abundant NH_3 in China enhances atmospheric HONO production by promoting the heterogeneous reaction of SO_2 with NO_2. *Environ Sci Technol*. 2019;53(24):14339–14347.
14. Ma Q, Zhong C, Ma J, Ye C, Zhao Y, Liu Y, Zhang P, Chen T, Liu C, Chu B, et al. Comprehensive study about the photolysis of nitrates on mineral oxides. *Environ Sci Technol*. 2021;55(13):8604–8612.
15. Xu W, Kuang Y, Zhao C, Tao J, Zhao G, Bian Y, Yang W, Yu Y, Shen C, Liang L, et al. NH_3-promoted hydrolysis of NO_2 induces explosive growth in HONO. *Atmos Chem Phys*. 2019;19(16):10557–10570.
16. Kebede MA, Varner ME, Scharko NK, Gerber RB, Raff JD. Photooxidation of ammonia on TiO_2 as a source of NO and NO_2 under atmospheric conditions. *J Am Chem Soc*. 2013;135(23):8606–8615.
17. Xu W, Zhao Y, Wen Z, Chang Y, Pan Y, Sun Y, Ma X, Sha Z, Li Z, Kang J, et al. Increasing importance of ammonia emission abatement in $PM_{2.5}$ pollution control. *Sci Bull*. 2022;67(17):1745–1749.
18. Sun Y, Gu B, van Grinsven HJM, Reis S, Lam SK, Zhang X, Chen Y, Zhou F, Zhang L, Wang R, et al. The warming climate aggravates atmospheric nitrogen pollution in Australia. *Research*. 2021;2021:9804583.
19. Krupa SV. Effects of atmospheric ammonia (NH_3) on terrestrial vegetation: A review. *Environ Pollut*. 2003;124(2):179–221.
20. Bhattarai N, Wang S, Pan Y, Xu Q, Zhang Y, Chang Y, Fang Y. $^{\delta}$15N-stable isotope analysis of NHx: An overview on

analytical measurements, source sampling and its source apportionment. *Front Environ Sci Eng*. 2021;15(6):126.
21. Zhou C, Li B, Zhang J, Henkelman G, Francisco JS, Li L. Resolving the amine-promoted hydrolysis mechanism of N_2O_5 under tropospheric conditions. *Proc Natl Acad Sci USA*. 2022;119(39):Article e2205668119.
22. Mount GH, Rumburg B, Havig J, Lamb B, Westberg H, Yonge D, Johnson K, Kincaid R. Measurement of atmospheric ammonia at a dairy using differential optical absorption spectroscopy in the mid-ultraviolet. *Atmos Environ*. 2002;36(11):1799–1810.
23. Sutton MA, Erisman JW, Dentener F, Möller D. Ammonia in the environment: From ancient times to the present. *Environ Pollut*. 2008;156(3):583–604.
24. He C-F, Wang X, Sun Y-Q, Pan X-M, Tao F-M. Theoretical study of the gaseous hydrolysis of NO_2 in the presence of amines. *J Phys Chem A*. 2017;121(1):226–237.
25. Li L, Duan Z, Li H, Zhu C, Henkelman G, Francisco JS, Zeng XC. Formation of HONO from the NH_3-promoted hydrolysis of NO_2 dimers in the atmosphere. *Proc Natl Acad Sci USA*. 2018;115(28):7236–7241.
26. Kebede MA, Scharko NK, Appelt LE, Raff JD. Formation of nitrous acid during ammonia photooxidation on TiO_2 under atmospherically relevant conditions. *J Phys Chem Lett*. 2013;4(16):2618–2623.
27. Rubasinghege G, Grassian VH. Role(s) of adsorbed water in the surface chemistry of environmental interfaces. *Chem Commun*. 2013;49(30):3071–3094.
28. Guo W, Zheng N, Zhang Z. Stable nitrogen isotopic signatures reveal the NH_4^+ evolution processes in pollution episodes in urban southwestern China. *Atmos Res*. 2021;253: Article 105474.
29. Wu C, Zhang S, Wang G, Lv S, Li D, Liu L, Li J, Liu S, Du W, Meng J, et al. Efficient heterogeneous formation of ammonium nitrate on the saline mineral particle surface in the atmosphere of East Asia during dust storm periods. *Environ Sci Technol*. 2020;54(24):15622–15630.
30. Gu C, Cui S, Ge X, Wang Z, Chen M, Qian Z, Liu Z, Wang X, Zhang Y. Chemical composition, sources and optical properties of nitrated aromatic compounds in fine particulate matter during winter foggy days in Nanjing, China. *Environ Res*. 2022;212:Article 113255.
31. Relph RA, Guasco TL, Elliott BM, Kamrath MZ, McCoy AB, Steele RP, Schofield DP, Jordan KD, Viggiano AA, Ferguson EE, et al. How the shape of an H-bonded network controls proton-coupled water activation in HONO formation. *Science*. 2010;327(5963):308–312.
32. Wang H, Sun Y, Dong F. Insight into the overlooked photochemical decomposition of atmospheric surface nitrates triggered by visible light. *Angew Chem Int Ed*. 2022;61(43):Article e202209201.
33. Ma S, Li Q, Zhang Y. A comprehensive study on hygroscopic behaviour and nitrate depletion of NaNO3 and dicarboxylic acid mixtures: Implications for nitrate depletion in tropospheric aerosols. *Atmos Chem Phys*. 2022;22(16):10955–10970.
34. Ebert M, Inerle-Hof M, Weinbruch S. Environmental scanning electron microscopy as a new technique to determine the hygroscopic behaviour of individual aerosol particles. *Atmos Environ*. 2002;36(39):5909–5916.
35. Li Q, Ma S, Liu Y, Wu X, Fu H, Tu X, Yan S, Zhang L, George C, Chen J. Phase state regulates photochemical HONO production from $NaNO_3$/dicarboxylic acid mixtures. *Environ Sci Technol*. 2024;58(17):7516–7528.
36. Hadjiivanov KI. Identification of neutral and charged NxOy surface species by IR spectroscopy. *Catal Rev*. 2000;42(1-2): 71–144.
37. Wu L, Tong S, Ge M. Heterogeneous reaction of NO_2 on Al_2O_3: The effect of temperature on the nitrite and nitrate formation. *J Phys Chem A*. 2013;117(23):4937–4944.
38. Sedlmair C, Seshan K, Jentys A, Lercher JA. Elementary steps of NOx adsorption and surface reaction on a commercial storage–reduction catalyst. *J Catal*. 2003;214(2):308–316.
39. Wang H, Hu Z, Liu S, Zhang X, Sun Y, Dong F. Dissecting the photochemical reactivity of metal ions during atmospheric nitrate transformations on photoactive mineral dust. *Environ Sci Technol*. 2024;58(28):12554–12562.
40. Chu B, Liu Y, Li H, Jia Y, Liu J, Cao Q, Chen T, Zhang P, Ma Q, Zeng XC, et al. Photocatalytic oxidation of NO_2 on TiO_2: Evidence of a new source of N_2O_5. *Angew Chem Int Ed*. 2023;62(25):Article e202304017.
41. Cao Q, Chu B, Zhang P, Ma Q, Ma J, Liu Y, Liu J, Zhao Y, Zhang H, Wang Y, et al. Effects of SO_2 on NH_4NO_3 photolysis: The role of reducibility and acidic products. *Environ Sci Technol*. 2023;57(23):8671–8679.
42. Wang D, Zhang L, Kamasamudram K, Epling WS. In situ-DRIFTS study of selective catalytic reduction of NOx by NH_3 over cu-exchanged SAPO-34. *ACS Catal*. 2013;3(5):871–881.
43. Gankanda A, Grassian VH. Nitrate photochemistry in NaY zeolite: Product formation and product stability under different environmental conditions. *J Phys Chem A*. 2013;117(10):2205–2212.
44. Ren Q, He Y, Wang H, Sun Y, Dong F. Rapid energy exchange between in situ formed bromine vacancies and CO_2 molecules enhances CO_2 photoreduction. *Research*. 2023;6:0244.
45. He Y, Sheng J, Ren Q, Sun Y, Hao W, Dong F. Operando identification of dynamic photoexcited oxygen vacancies as true catalytic active sites. *ACS Catal*. 2023;13(1):191–203.
46. Zhang X, Tong S, Jia C, Zhang W, Wang Z, Tang G, Hu B, Liu Z, Wang L, Zhao P, et al. Elucidating HONO formation mechanism and its essential contribution to OH during haze events. *npj Clim Atmos Sci*. 2023;6(1):55.
47. Fu X, Wang T, Zhang L, Li Q, Wang Z, Xia M, Yun H, Wang W, Yu C, Yue D, et al. The significant contribution of HONO to secondary pollutants during a severe winter pollution event in southern China. *Atmos Chem Phys*. 2019;19(1):1–14.